Department of Aerospace Engineering

EXPERIMENTS ON THE **INSTABILITIES IN SWIRLING AND NON-SWIRLING FREE JETS**

A Thesis in

Aerospace Engineering

by

Jayanta Panda

Submitted in Partial Fulfillment
of the Requirements
for the Degree of

Doctor of Philosophy

December 1990

We approve the thesis of Jayanta Panda.

Date of Signature:

Dennis K McLaughlin — Oct 12, 1990

Dennis K. McLaughlin
Professor of Aerospace Engineering
Head of the Department of Aerospace Engineering
Thesis Adviser
Chair of Committee

Philip J. Morris — Oct 9, 1990

Philip J. Morris
Professor of Aerospace Engineering

John M. Cimbala — Oct 11, 1990

John M. Cimbala
Associate Professor of Mechanical Engineering

Gary S. Settles — Oct. 1, 1990

Gary S. Settles
Professor of Mechanical Engineering

Stephen R. Turns — Oct. 11/ 1990

Stephen R. Turns
Professor of Mechanical Engineering

ABSTRACT

Instabilities present in a free-swirling jet in the Reynolds number range from 20,000 to 60,000 and swirl number of *0.45* were studied experimentally, using smoke visualization and hot-wire measurements. A non-swirling jet of Reynolds number 60,000 produced from the same facility was also studied for validation of the experimental procedures and direct comparison with the swirling jet. To the author's knowledge this represents the first study of the instabilities of a swirling free jet reported in the open literature.

Time-mean velocity components and turbulence intensity were surveyed using a single hot-wire (non-swirling jet) and a V-wire (swirling jet) probe. Like the non-swirling jet, the young shear layer from the nozzle exit of the swirling jet develops Kelvin-Helmholtz instability waves, which roll up into large scale organized motion.

To enhance our understanding of these instabilities, axisymmetric and helical waves were excited in the Strouhal number range 0.75-1.5 (swirling jet) and 0.9-3.75 (non-swirling jet) by acoustic excitation. Phase-locked multiple exposure photographs confirmed the existence of such structures. Velocity spectra and ensemble averaged measurements (phase referenced to the excitation) were used to determine the axial evolution of the large-scale structures. These measurements were compared with the instability wave evolution in non-swirling jets obtained using Michalke's calculation. In the swirling jets, the growth rates of the helical mode are higher than those of the

axisymmetric mode. However, the growth rates of all instability waves are considerably smaller in a swirling jet than in a non-swirling jet. In general, swirl stabilizes the organized motions.

Another important phenomenon appearing at the core of a free-swirling jet is vortex bursting. Both spiral and bubble type vortex breakdown are observed at the jet core. Vortex bursting induces an asymmetric flowfield and instantly replaces the potential core with a large amount of turbulence. Upon interacting with the vortex breakdown, the shear layer along the jet periphery loses its organized structure and, in general, “random turbulence” follows.

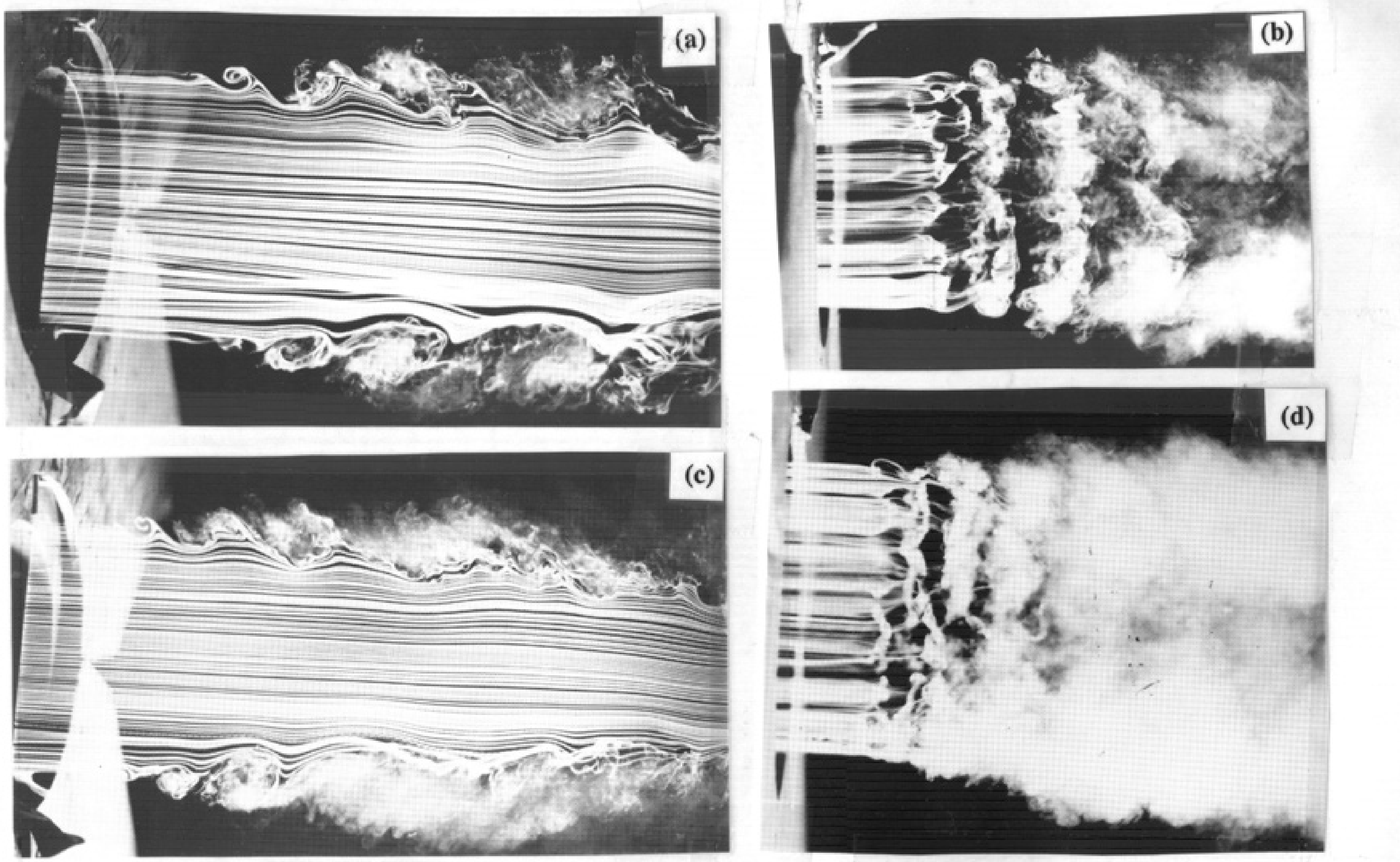

Figure 3.10. Natural non-swirling jet photographs. (a) Straight wire, Re = 29,000; (b) Circular wire, Re = 29,000; (c) Straight wire, Re = 60,000; (d) Circular wire, Re = 60,000.

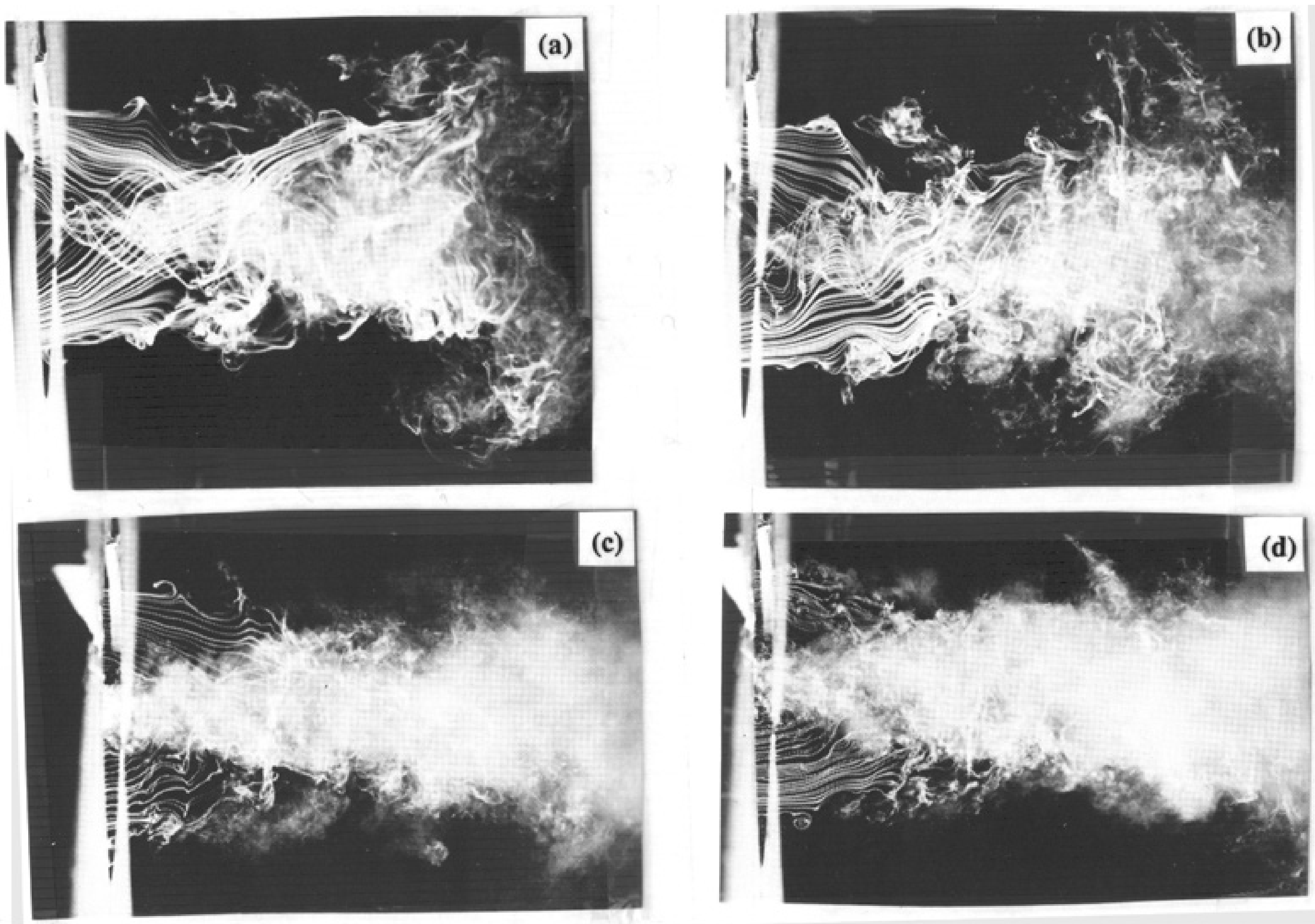

Figure 3.11. Natural swirling jet photographs. All photographs are produced using straight smoke wire. (a) Re = 15,000; (b) Re = 20,000; (c) Re = 40,000; (d) Re = 57,000.

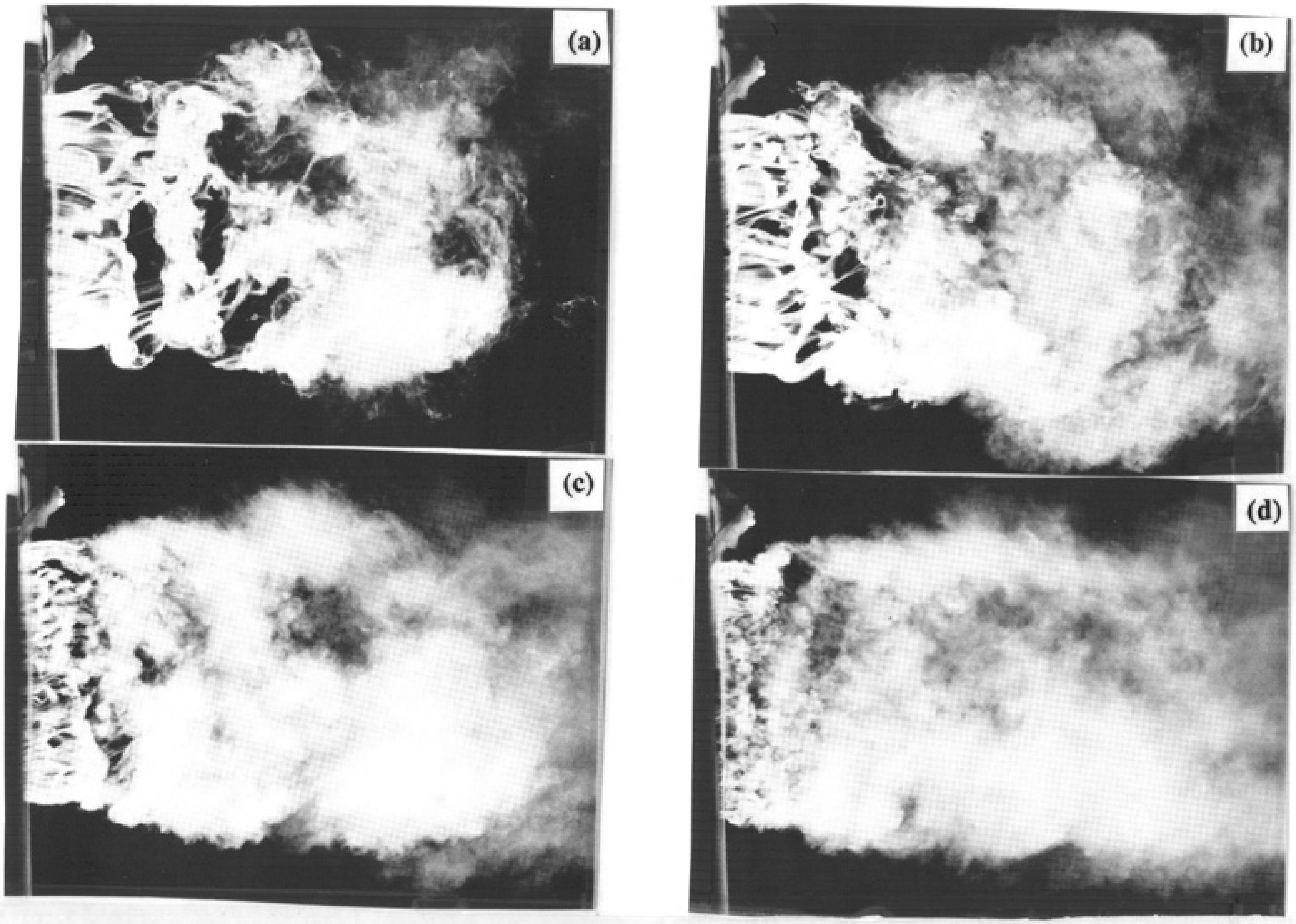

Figure 3.12. Natural swirling jet photographs. All photographs are produced using a circular smoke wire. (a) Re = 15,000; (b) Re = 22,000; (c) Re = 40,000; (d) Re = 60,000.

Figure 3.13. Asymmetry of the flowfield produced by vortex bursting. Re = 15,000.

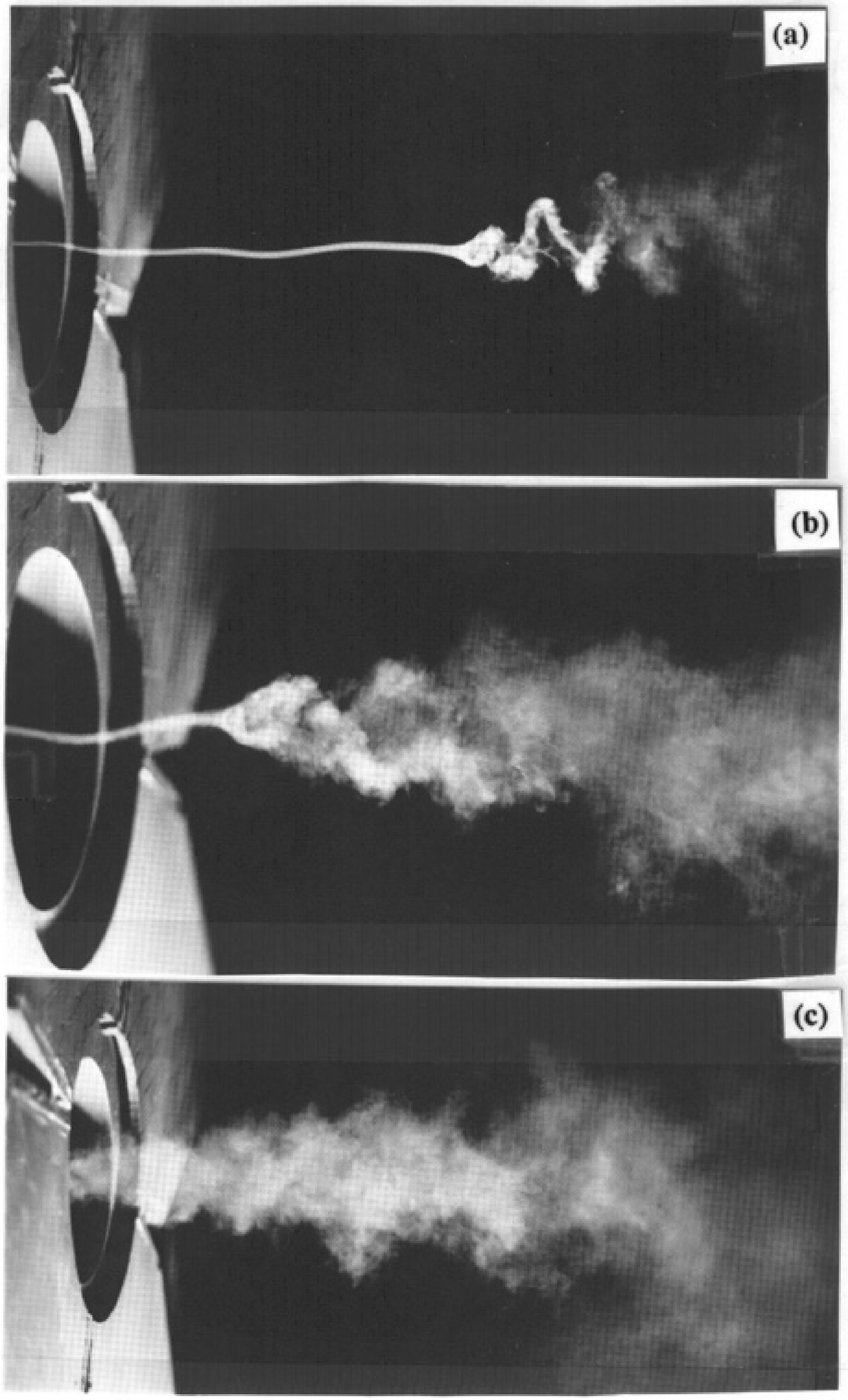

Figure 3.14. Vortex bursting at various Reynolds no. Swirling jet; (a) Re = 14,000; (b) Re = 25,000; (c) Re = 40,000.

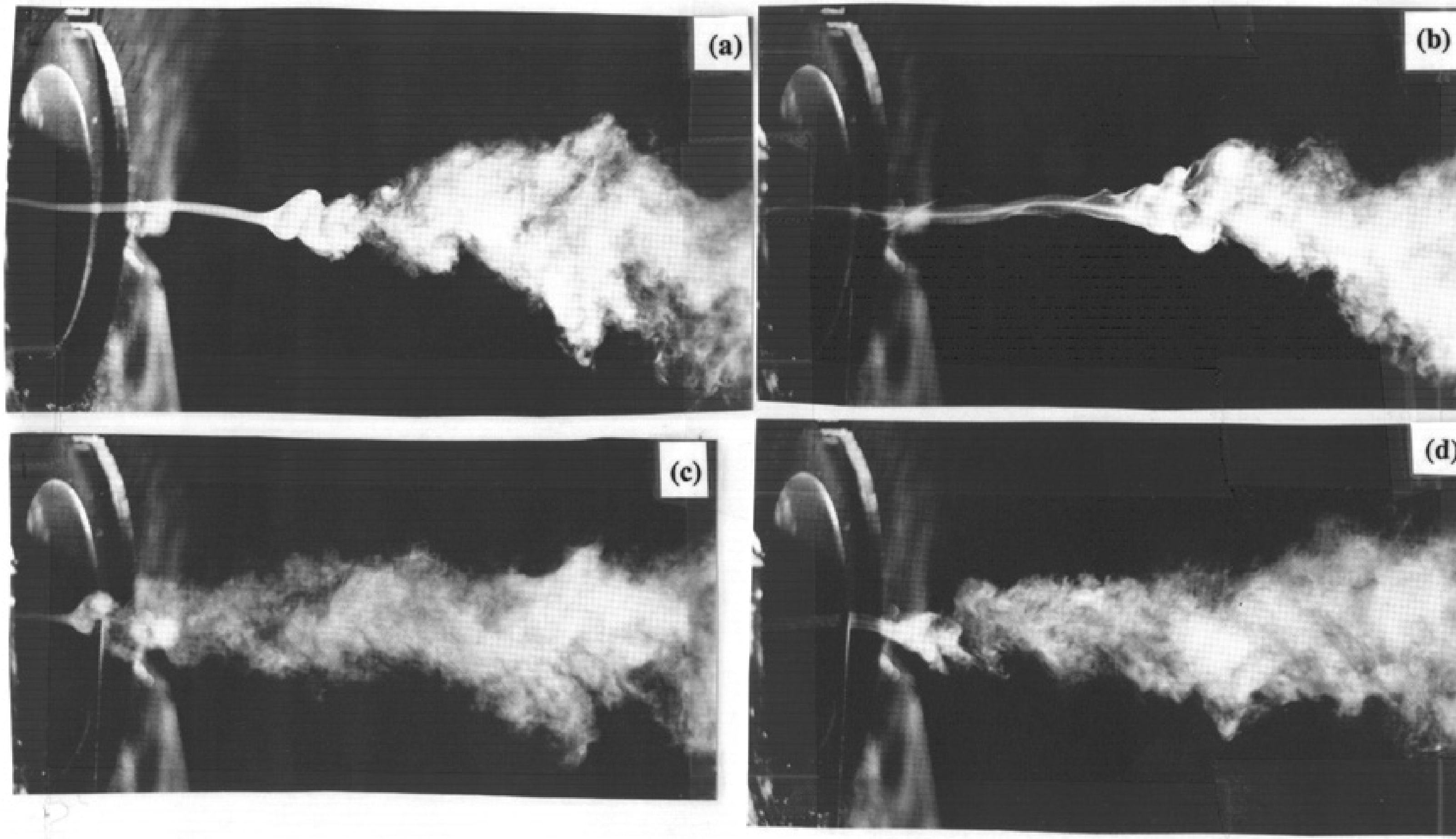

Figure 3.15. Probe interference effect on the vortex bursting location. All photographs at Re = 25,000. (a) without a probe; (b) probe is at $x/D = 0.2$, $r/D = 0.3$; (c) and (d) probe is at $x/D = 0.2$, $r/D = 0.5$ (jet centerline).

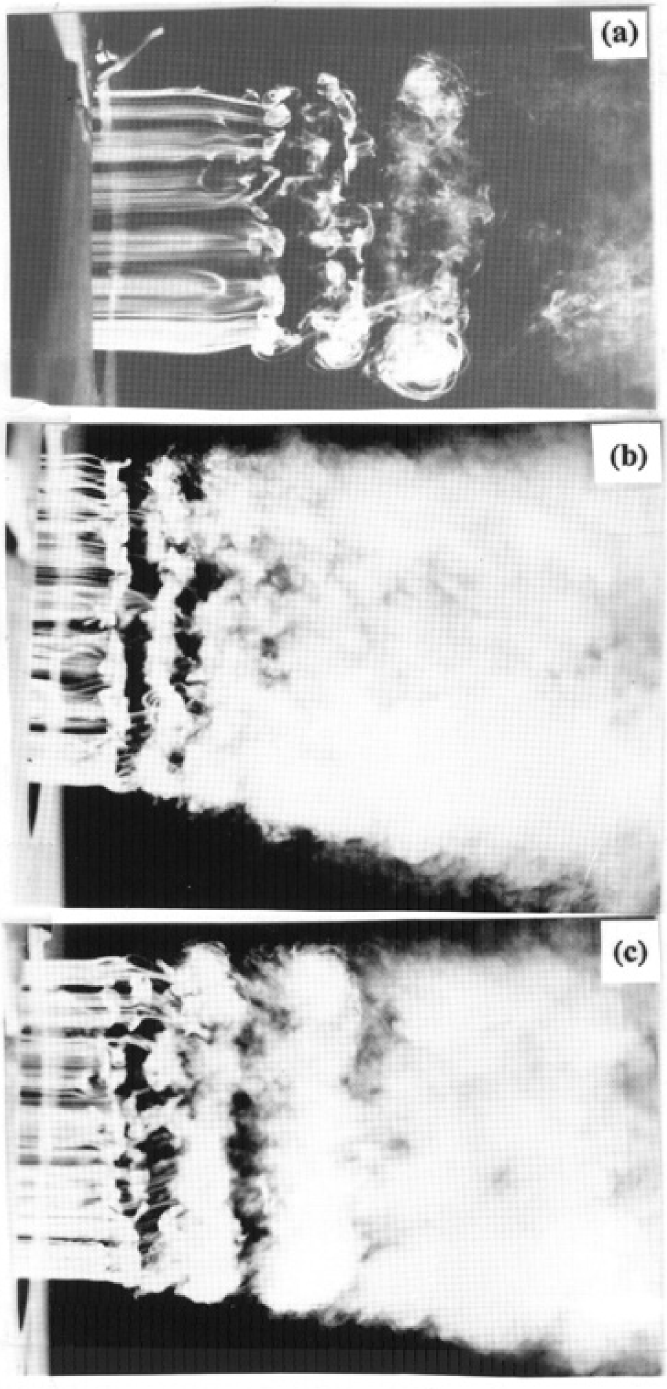

Figure 3.16. Single exposure photograph of the axisymmetric instability waves in excited non-swirling jets. (a) Re = 29,000, St. = 1.1, 76 dB; (b) Re = 60,000, St = 3.75, 80 dB; (c) Re = 60,000, St. = 1.88, 80 dB.

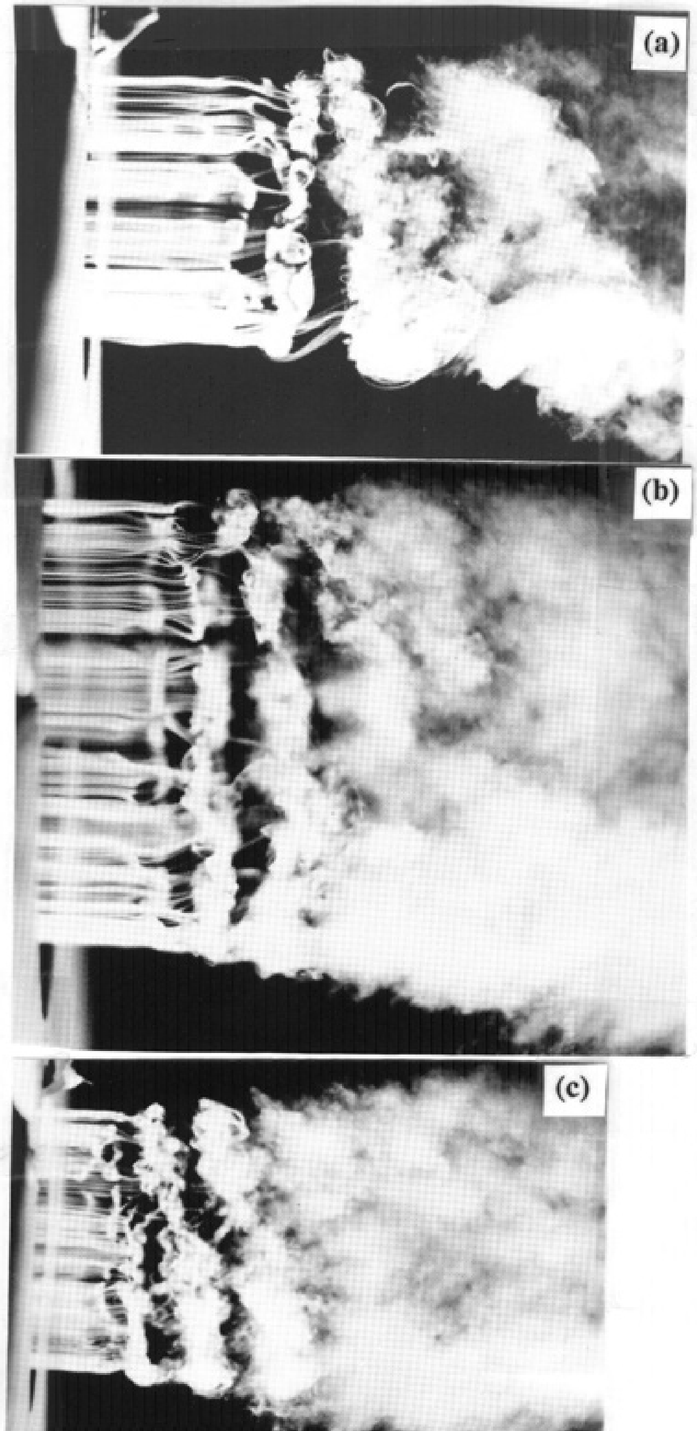

Figure 3.17. Single exposure photographs of the helical instability waves in excited non-swirling jets. (a) Re = 29,000, St. = 1.1, 76 dB; (b) Re = 60,000, St. = 3.75, 80 dB; (c) Re = 60,000, St. = 1.88, 80 dB.

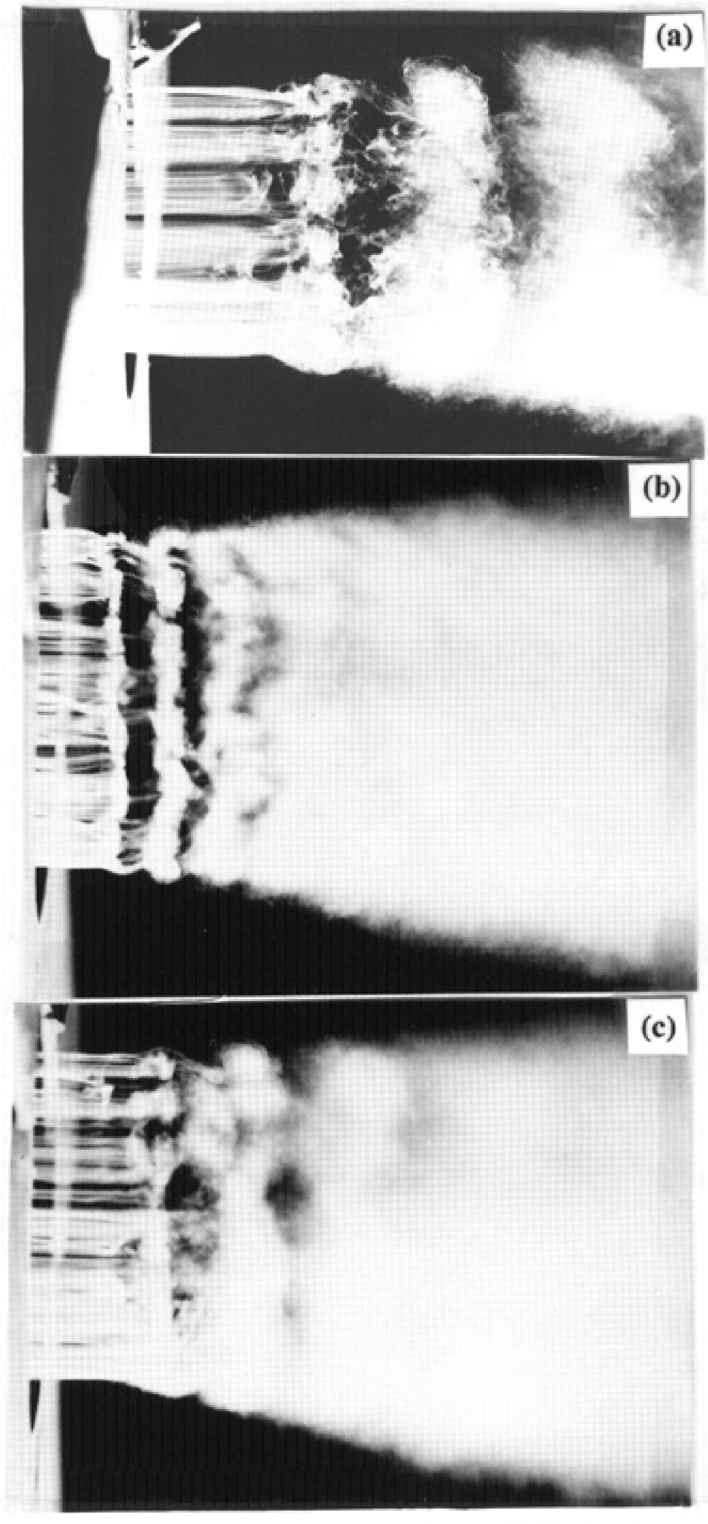

Figure 3.18. phase locked multiple exposure photographs of the axisymmetric modes in non-swirling jets. (a) Re = 29,000, St. = 1.1, 15 exposures; (b) Re = 60,000, St. = 3.75, 15 exposures; (c) Re = 60,000, St. = 1.88, 15 exposures.

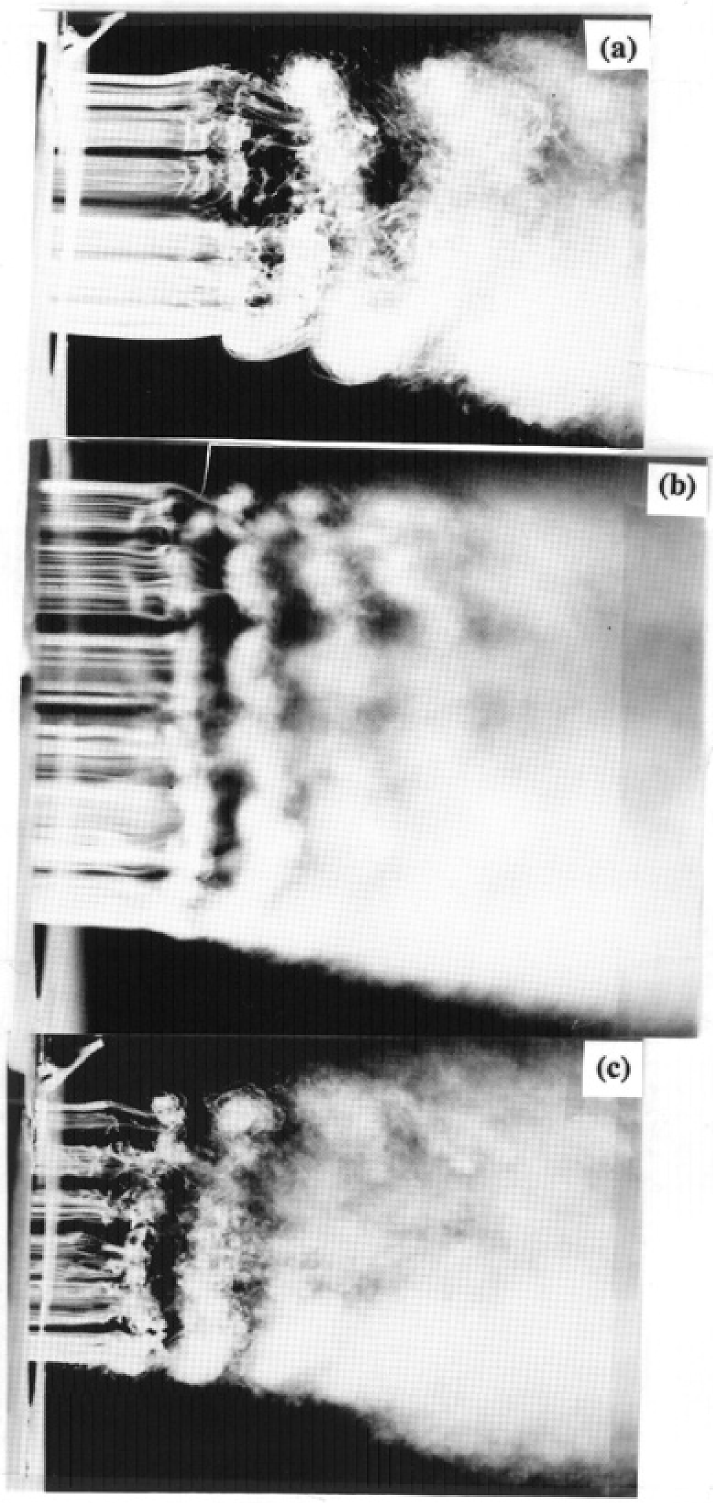

Figure 3.19. Phase locked multiple exposure photographs of the helical mode in non-swirling jets. (a) Re = 29,000, St. = 1.1, 15 exposures; (b) Re = 60,000, St. = 3.75, 15 exposures; (c) Re = 60,000, St. = 1.88, 17 exposures.

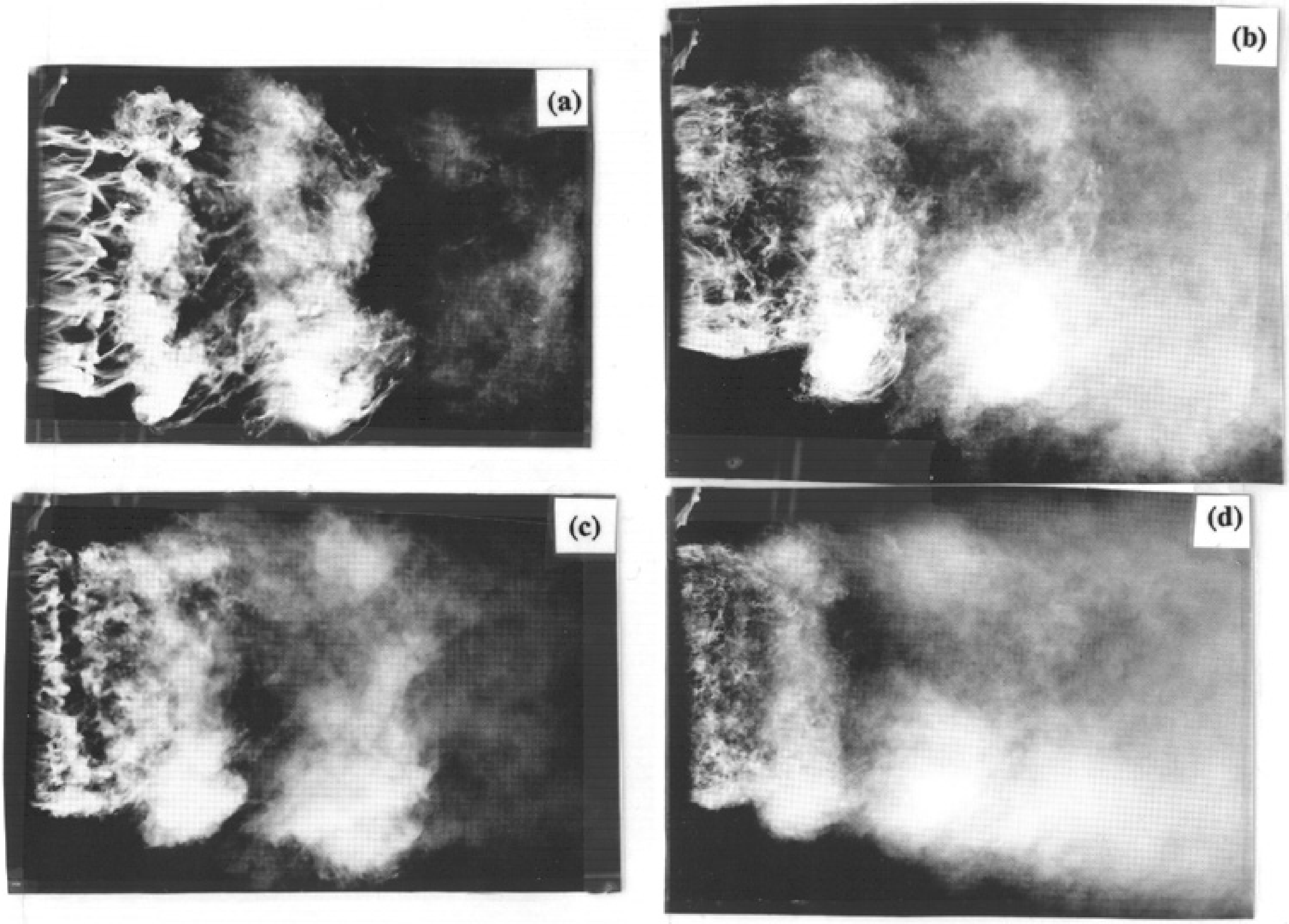

Figure 3.20. Excited (axisymmetric mode) swirling jet photographs. (a) single exposure, Re = 22,000, St. = 1.0 (14.5 Hz.), 86 dB; (b) multiple (10) exposures, Re = 22,000, St. = 1.0; (c) single exposure, Re = 40,000, St. = 1.25 (33 Hz.), 90 dB; (d) multiple (16) exposures, Re = 40,000, St. = 1.25.

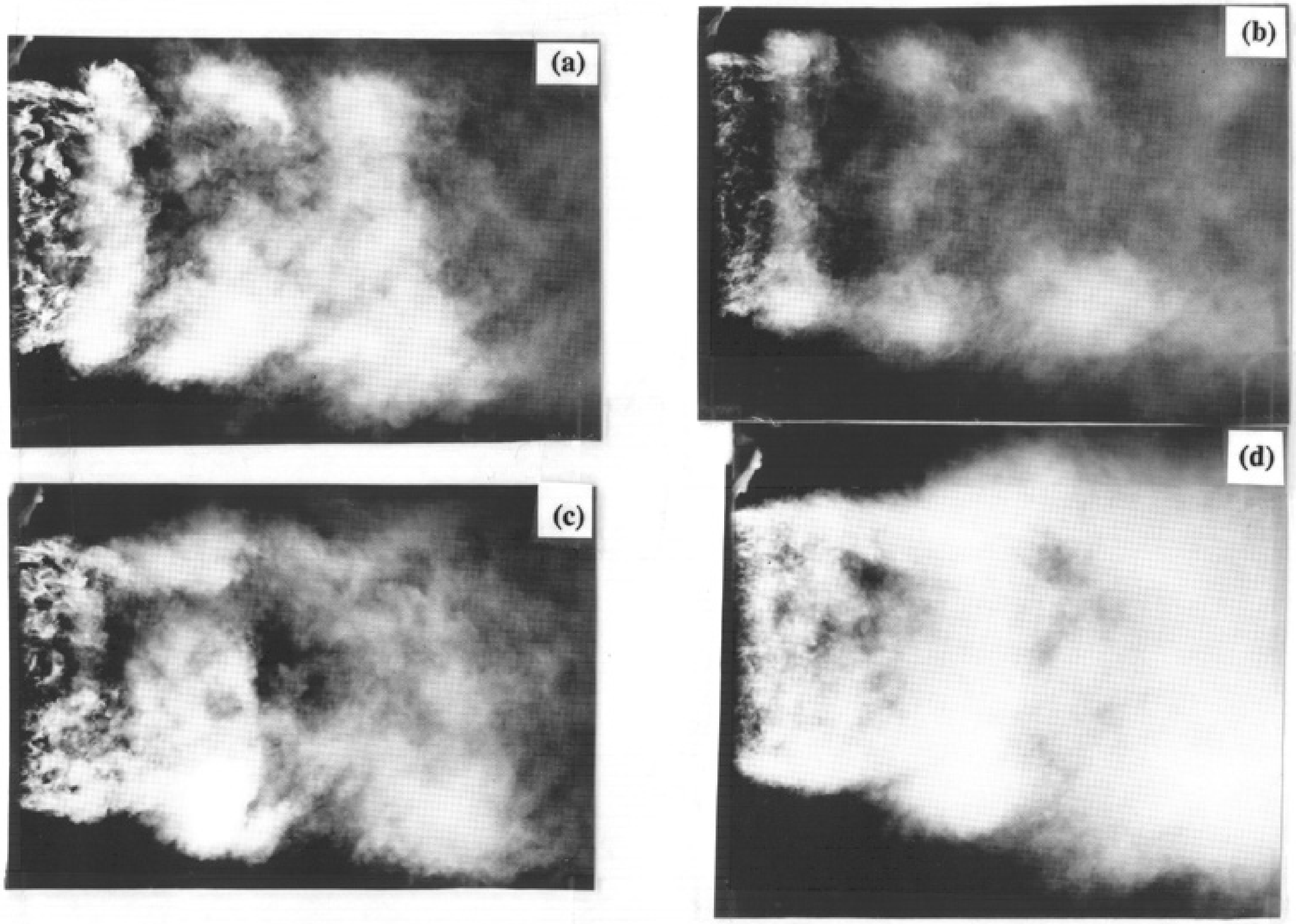

Figure 3.21. Photographs of the axisymmetric mode of excitation of the Re 60,000 swirling jet. (a) single exposure, St. = 1.5 (56 Hz.), 100 dB; (b) multiple (14) exposures, St. = 1.5; (c) single exposure; St. = 0.75 (28 Hz.), 100 dB; (d) multiple (11) exposures, St. = 0.75.

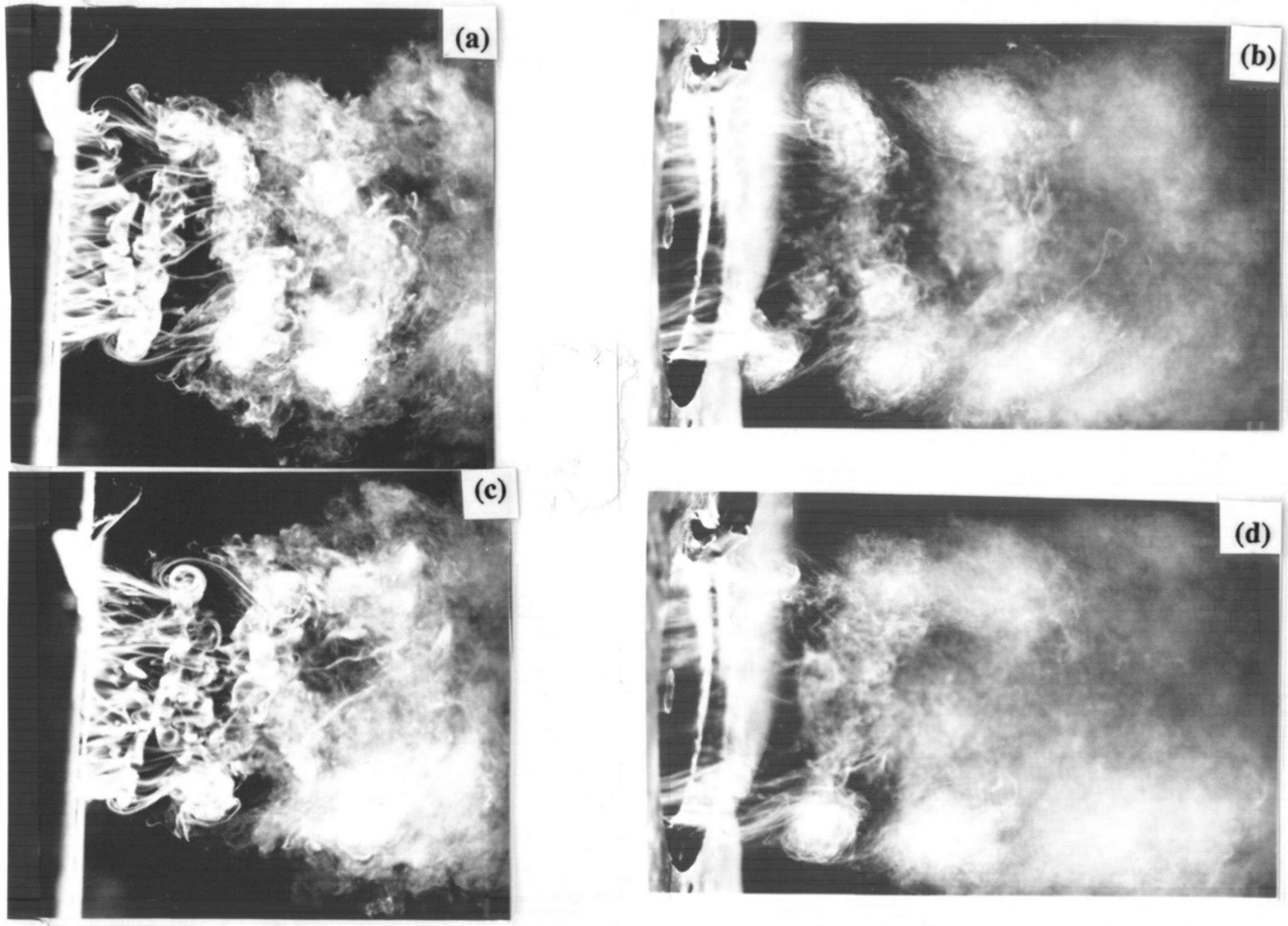

Figure 3.22. Photographs of the helical modes of excitation of the Re = 21,000 swirling jets. (a) Single exposure, m = -1 mode, St. = 1.2 (17 Hz.), 86 dB; (b) multiple (17) exposures, m = -1 mode, St. = 1.2; (c) single exposure, m = +1, St. = 1.2, 86 dB; (d) multiple (17) exposures, m = +1, St. = 1.2.